Indian Journal of Pure & Applied Physics
Vol. 55, April 2017, pp. 275-283

Dual solution of unsteady separated stagnation-point flow in a nanofluid with suction: A finite element analysis

Rajesh Sharma[a,b]*, Anuar Ishak[b] & Ioan Pop[c]

[a]Department of Mathematics, National Institute of Technology Hamirpur, Hamirpur 177 005, India

[b]School of Mathematical Sciences, Faculty of Science and Technology, Universiti Kebangsaan Malaysia 43600, Malaysia

[c]Department of Mathematics, Babeş-Bolyai University 400 084, Romania

Received 1 February 2013; revised 19 February 2014; accepted 6 April 2014

Unsteady two-dimensional stagnation-point flow of a viscous and incompressible fluid filled by a nanofluid over a permeable flat plate with suction has been investigated numerically. The mathematical model used for the nanofluid incorporates the effect of Brownian motion and thermophoresis. The velocity of the ambient (inviscisd) fluid has been assumed to vary linearly with the distance from the stagnation-point. The resulting non-linear governing equations with associated boundary conditions have been solved numerically using finite element method (FEM). The effect of the unsteadiness parameter A, mass suction parameter s, Lewis number Le, the Brownian motion parameter Nb and the thermophoresis parameter Nt on the flow, temperature and nanoparticle concentration in the boundary layer region have been analyzed graphically. The impact of the unsteadiness parameter and mass suction/injection parameter on the skin friction, rate of heat transfer and mass transfer have been examined and discussed. Interesting observation is that dual solutions exist for a certain range of the suction/injection parameter, and this range decreases with increasing values of the unsteadiness parameter.

Keywords: Nanofluid, Stagnation-point flow, Heat transfer, Dual solutions, FEM

1 Introduction

A stagnation-point flow develops, when an external flow impinges on a surface of a submerged body in a fluid flow, the streamline of the flow being perpendicular to the surface of the body. Great attention has been done in fluid dynamics to the study of stagnation-point flows because of their importance in many engineering applications, such as, for example, cooling of electronic devices by fans, cooling of nuclear reactors, and many hydrodynamics processes. Hiemenz[1] was the first to study the steady two- dimensional stagnation-point flow on a flat plate using a similarity transformation to reduce the Navier-Stokes equations to a nonlinear ordinary differential equation. It was later extended to axisymmetric case by Homann[2]. Further, the effects of suction/injection on the Hiemenz flow problem have been introduced[3,4]. On the other hand, the study of heat transfer in stagnation-point flow has also been considered by many authors[5–8] in the hydrodynamic case. An excellent description of this problem can be found in the books by Bejan[9], Schlichting and Gersten[10], Leal[11], Pop and Ingham[12], etc.

Ma and Hui[13] obtained the similarity solution of the unsteady two-dimensional stagnation-point flow of an incompressible viscous fluid over a flat plate using Lie group transformation method. They observed that the solution of Hiemenz flow problem is not unique. This problem has two solutions, one representing an attached flow and the other a reverse flow. It is pointed out in the excellent book by Telionis[14] that unsteady flows are those whose properties depend on time if references with respect to an Eulerian frame. The peculiar distinction between steady and unsteady motion in fluid mechanics has no counterpart in solid-mechanics problems. Examples of unsteady flows are many. In fact, there is no actual flow situation, natural or artificial, that does not involve unsteadiness. The helicopter rotor, the cascades of blades of turbomachinery, and the ship propeller normally operate in an unsteady aerodynamic environment[14].

In many industries such as power, manufacturing and transportation etc, fluids such as water, ethylene glycol, engine oil etc are commonly used as for cooling any sort of high energy device. But, these fluids have limited heat transfer capabilities due to their low heat transfer properties. So, effective cooling techniques are greatly needed. The term

*Corresponding author (E-mail: raj.juit@gmail.com)

"nanofluid" was first proposed by Choi[15] describes a liquid composed of metals nanoparticles (diameter less than 50 nm) dispersed in a base fluid. The nanofluid has thermal conductivity up to three times higher than the base fluid. Nanofluid is envisioned to describe a fluid in which nanometer-sized particles are suspended in conventional heat transfer basic fluids. Conventional heat transfer fluids, including oil, water, and ethylene glycol mixture are poor heat transfer fluids, since the thermal conductivity of these fluids play important role on the heat transfer coefficient between the heat transfer medium and the heat transfer surface. Therefore numerous methods have been taken to improve the thermal conductivity of these fluids by suspending nano/micro or larger-sized particle materials in liquids[16]. The comprehensive survey on nanofluids has been reported elsewhere[17-23]. It is worth mentioning that Buongiorno[24], and Tiwari and Das[25] have proposed two different models to study the flows of nanofluid, which was recently used by many researchers[26-43]. In this paper, we extend the work by Ma and Hui[13] to the heat transfer analyses in a nanofluid using the mathematical nanofluid model proposed by Buongiorno[24]. It is worth mentioning that some researchers[26-31] have assumed that nanoparticles are suspended in the nanofluid using either surfactant or surface charge technology. This prevents particles from agglomeration and deposition on the porous matrix.

The objective of this paper is to investigate the heat transfer characteristics caused by the stagnation-point flow of a nanofluid over a permeable flat plate using finite element method. The dual solutions are obtained and the results for the skin friction coefficient, local Nusselt number, local Sherwood number, velocity and temperature profiles as well as the nanoparticle concentration profiles are discussed for different values of the governing parameters. A review of the literature shows that no attempt has been taken to solve the problem that we are considering in this paper. Thus, we are confident that this problem is original and the results are new and very important for the fluid mechanics and heat transfer researchers.

2 Problem Formulations

Consider the unsteady two-dimensional stagnation-point flow of a viscous and incompressible nanofluid over a permeable flat plate. Following Ma and Hui[13] it is assumed that the free stream velocity is $u_e(x,t) = A(x/t)$, where, A is a positive constant, t is the time and x is the axis measured along the plate. It is also assumed that the temperature and the nanoparticle fraction at the plate take constant values T_w and C_w, respectively, while the ambient values are denoted by T_∞ and C_∞, respectively. Under these assumptions, it can be shown that the unsteady boundary layer equations of mass, momentum, thermal energy, and nanoparticles for nanofluids can be written in Cartesian coordinates x and y as, see Ma and Hui[13], and Kuznetsov and Nield[30]:

$$\frac{\partial u}{\partial x}+\frac{\partial v}{\partial y}=0 \qquad \ldots (1)$$

$$\frac{\partial u}{\partial t}+u\frac{\partial u}{\partial x}+v\frac{\partial u}{\partial y}=\frac{\partial u_e}{\partial t}+u_e\frac{\partial u_e}{\partial x}+\nu\frac{\partial^2 u}{\partial y^2} \qquad \ldots (2)$$

$$\frac{\partial T}{\partial t}+u\frac{\partial T}{\partial x}+v\frac{\partial T}{\partial y}=\alpha\frac{\partial^2 T}{\partial y^2}+\tau\left[D_B\frac{\partial C}{\partial y}\frac{\partial T}{\partial y}+\left(\frac{D_T}{T_\infty}\right)\left(\frac{\partial T}{\partial y}\right)^2\right] \qquad \ldots (3)$$

$$\frac{\partial C}{\partial t}+u\frac{\partial C}{\partial x}+v\frac{\partial C}{\partial y}=D_B\frac{\partial^2 C}{\partial y^2}+\left(\frac{D_T}{T_\infty}\right)\frac{\partial^2 T}{\partial y^2} \qquad \ldots (4)$$

where y is the coordinate measured in the direction normal to the plate, u and v are the velocity components along the $x-$and $y-$ axes, T is the nanofluid temperature, C is the nanoparticle fraction, α is the thermal diffusivity, ν is the kinematic viscosity, D_B is the Brownian diffusion coefficient, D_T is the thermophoretic diffusion coefficient and $\tau=(\rho c)_p/(\rho c)_f$ with ρ being the density, c is volumetric volume expansion coefficient and ρ_p is the density of the particles. The initial and boundary conditions of these equations are:

$$\begin{aligned} &t\le 0: \quad u=v=0, \quad T=T_\infty, \quad C=C_\infty \quad \text{for any } x, y\\ &t>0: \quad v=v_w(x,t), \quad u=0, \quad T=T_w, \quad C=C_w \quad \text{at} \quad y=0\\ &\qquad\quad u=u_e(x,t)=A\,(x/t), \quad T=T_\infty, \quad C=C_\infty \quad \text{as} \quad y\to\infty \end{aligned} \qquad \ldots (5)$$

where $v_w(x,t)=-A(\nu/t)^{1/2}s$ is the mass flux velocity with $v_w(x,t)<0$ corresponding to suction and $v_w(x,t)>0$ corresponding to injection or blowing.

Following Ma and Hui[13], we introduce the following similarity transformation:

$$u=A(x/t)f'(\eta),\quad v=-A(\nu/t)^{1/2}f(\eta),\quad \theta(\eta)=(T-T_\infty)/(T_w-T_\infty)$$
$$\phi(\eta)=(C-C_\infty)/(C_w-C_\infty),\quad \eta=y\sqrt{1/\nu t} \qquad \ldots (6)$$

where primes denote differentiation with respect to η. Using transformation Eq. (6), Eq. (1) is automatically satisfied, while Eqs (2), (3) and (4), respectively, reduce to the following nonlinear ordinary differential equations:

$$f'''+\left(Af+\frac{\eta}{2}\right)f''+(1-Af')f'+A-1=0 \qquad \ldots (7)$$

$$\frac{1}{\Pr}\theta''+Af\theta'+Nb\,\theta'\phi'+Nt\,\theta'^2+\frac{\eta}{2}\theta'=0 \qquad \ldots (8)$$

$$\phi''+A\,Le\,f\phi'+\frac{Nt}{Nb}\theta''+Le\frac{\eta}{2}\phi=0 \qquad \ldots (9)$$

Subject to the boundary conditions:

$$f(0)=s,\quad f'(0)=0,\quad \theta(0)=1,\quad \phi(0)=1$$
$$f'(\eta)\to 1,\quad \theta(\eta)\to 0,\quad \phi(\eta)\to 0\quad \text{as}\quad \eta\to\infty \qquad \ldots (10)$$

In Eq. (10), s is the suction/injection parameter with $s>0$ for suction and $s<0$ for injection. The remaining four parameters Pr, Le, Nb and Nt are the Prandtl number, Lewis number, the Brownian motion parameter and the thermophoresis parameter, respectively, and are defined by:

$$\Pr=\frac{\nu}{\alpha},\quad \mathrm{Le}=\frac{\nu}{\mathrm{D_B}},\quad Nb=\frac{(\rho c)_p D_B(C_w-C_\infty)}{(\rho c)_f\nu},\quad Nt=\frac{(\rho c)_p D_T(T_w-T_\infty)}{(\rho c)_f T_\infty\nu} \qquad \ldots (11)$$

It is important to note that this boundary value problem reduces to the classical problem of unsteady boundary layer flow and heat transfer near the stagnation-point of a viscous and incompressible fluid (regular fluid) when Nb and Nt are all zero in Eqs (8) and (9).

Physical quantities of interest are the skin friction coefficient C_f, the local Nusselt number (Nu_x) and the local Sherwood number (Sh_x), , which are defined as:

$$C_f=\frac{\tau_w}{\rho u_e^2},\quad Nu_x=\frac{x\,q_w}{k(T_w-T_\infty)},\quad Sh_x=\frac{x\,j_w}{D_B(C_w-C_\infty)} \qquad \ldots (12)$$

where τ_w is the surface shear stress, q_w is the surface heat flux and j_w is the concentration flux at the plate, and are given by:

$$\tau_w=\mu\left(\frac{\partial u}{\partial y}\right)_{y=0},\quad q_w=-k\left(\frac{\partial T}{\partial y}\right)_{y=0},\quad j_w=-D_B\left(\frac{\partial C}{\partial y}\right)_{y=0} \qquad \ldots (13)$$

Using the similarity variables Eq. (6) , we obtain:

$$Re_x^{1/2}C_f=f''(0),\ Re_x^{-1/2}Nu_x=-\theta'(0),\ Re_x^{-1/2}Sh_x=-\varphi'(0) \qquad \ldots (14)$$

where $Re_x = u_e\,x/\nu$ is the local Reynolds number.

For this flow, the streamlines ψ, isotherms $(T-T_\infty)/(T_w-T_\infty)$ and iso-concentration $(C-C_\infty)/(C_w-C_\infty)$ can be defined as:

$$\psi=\frac{A}{t^{1/2}}x\,f(y\sqrt{1/\nu t}),\quad (T-T_\infty)/(T_w-T_\infty)=\theta(y\sqrt{1/\nu t})$$
$$(C-C_\infty)/(C_w-C_\infty)=\phi(y\sqrt{1/\nu t}) \qquad \ldots (15)$$

where ψ is defined in the usual way as $u=\partial\psi/\partial y$ and $v=-\partial\psi/\partial x$.

The set of ordinary differential Eqs (7-10) are highly non-linear, and cannot be solved analytically. Therefore, the finite element method[44-47] is implemented to solve this system numerically. However, in order that we compare the present results with ones from the open literature, we consider the steady-state flow and heat transfer of a viscous and incompressible (regular) fluid near the stagnation-point of an impermeable semi-infinite flat plate, which are given by the following equations[9]:

$$f'''+f\,f''-f'^2+1=0 \qquad \ldots (16)$$

$$\frac{1}{Pr}\theta''+f\,\theta'=0 \qquad \ldots (17)$$

Subject to the boundary conditions

$$f(0)=0,\quad f'(0)=0,\quad \theta(0)=1$$
$$f'(\eta)\to 1,\quad \theta(\eta)\to 0\quad \text{as}\quad \eta\to\infty \qquad \ldots (18)$$

3 Method of Solution

3.1 Finite element method

The finite element method is a powerful technique for solving ordinary or partial differential equations as well as integral equations. The basic concept is that the whole domain is divided into smaller elements of finite dimensions called "finite elements". It is the most versatile numerical technique in modern engineering analysis and has been employed to study diverse problems in heat transfer, fluid mechanics, chemical processing, rigid body dynamics, solid mechanics, electrical systems, acoustics and many other fields.

For the solution of the system of simultaneous ordinary differential equations given by Eqs (7-9), with the boundary conditions Eq. (10) , we first assume:

$$f' = g \qquad \ldots (19)$$

The system of Eqs (7-9) then reduces to:

$$g'' + \left(A f + \frac{\eta}{2} \right) g' + (1 - A g) g + A - 1 = 0 \qquad \ldots (20)$$

$$\theta'' + Pr\, Af\, \theta' + Pr\, Nb \theta' \phi' + Pr\, Nt (\theta')^2 + Pr \frac{\eta}{2} \theta' = 0 \qquad \ldots (21)$$

$$\phi'' + ALef\, \phi' + \frac{Nt}{Nb} \theta'' + Le \frac{\eta}{2} \phi' = 0 \qquad \ldots (22)$$

and the corresponding boundary conditions now become:

$$\begin{aligned} &\eta = 0: \quad f = s,\ g = 0,\ \theta = 1,\ \phi = 1 \\ &\eta \to \infty:\ g = 1,\ \theta = 0,\ \phi = 0 \end{aligned} \qquad \ldots (23)$$

3.2 Variational formulation

The variational form associated with Eqs (19-22) over a typical linear element (η_e, η_{e+1}), is given by

$$\int_{\eta_e}^{\eta_{e+1}} w_1 \{ f' - g \} d\eta = 0 \qquad \ldots (24)$$

$$\int_{\eta_e}^{\eta_{e+1}} w_2 \left(g'' + \left(A f + \frac{\eta}{2} \right) g' + (1 - A g) g + A - 1 \right) d\eta = 0 \qquad \ldots (25)$$

$$\int_{\eta_e}^{\eta_{e+1}} w_3 \left(\theta'' + \Pr Af \theta' + \Pr Nb \theta' \phi' + \Pr Nt (\theta')^2 + \Pr \frac{\eta}{2} \theta' \right) d\eta = 0 \qquad \ldots (26)$$

$$\int_{\eta_e}^{\eta_{e+1}} w_4 \left(\phi'' + ALef \phi' + \frac{Nt}{Nb} \theta'' + Le \frac{\eta}{2} \phi' \right) d\eta = 0 \qquad \ldots (27)$$

where w_1, w_2, w_3 and w_4 are arbitrary test functions and may be viewed as the variation in f, g, θ and ϕ respectively.

3.3 Finite element formulation

The finite element model may be obtained from the above equations by substituting finite element approximations of the form:

$$f = \sum_{j=1}^{2} f_j \psi_j, \quad g = \sum_{j=1}^{2} g_j \psi_j, \quad \theta = \sum_{j=1}^{2} \theta_j \psi_j, \quad \phi = \sum_{j=1}^{2} \phi_j \psi_j \qquad \ldots (28)$$

with

$$w_1 = w_2 = w_3 = w_4 = \psi_i, \ (i = 1, 2) \qquad \ldots (29)$$

In our computations, the shape functions for a typical element (η_e, η_{e+1}) are taken as: linear element

$$\psi_1^e = \frac{(\eta_{e+1} - \eta)}{(\eta_{e+1} - \eta_e)}, \qquad \psi_2^e = \frac{(\eta - \eta_e)}{(\eta_{e+1} - \eta_e)}, \qquad \eta_e \le \eta \le \eta_{e+1} \qquad \ldots (30)$$

The finite element model of the equations thus formed is given by;

$$\begin{bmatrix} [K^{11}] & [K^{12}] & [K^{13}] & [K^{14}] \\ [K^{21}] & [K^{22}] & [K^{23}] & [K^{24}] \\ [K^{31}] & [K^{32}] & [K^{33}] & [K^{34}] \\ [K^{41}] & [K^{42}] & [K^{43}] & [K^{44}] \end{bmatrix} \begin{bmatrix} \{f\} \\ \{g\} \\ \{\theta\} \\ \{\phi\} \end{bmatrix} = \begin{bmatrix} \{b^1\} \\ \{b^2\} \\ \{b^3\} \\ \{b^4\} \end{bmatrix}$$

where $[K^{mn}]$ and $[b^m]$ $(m, n = 1, 2, 3, 4)$ are defined as:

$$K_{ij}^{11} = \int_{\eta_e}^{\eta_{e+1}} \psi_i \frac{\partial \psi_j}{\partial \eta} d\eta, \quad K_{ij}^{12} = -\int_{\eta_e}^{\eta_{e+1}} \psi_i \psi_j d\eta, \quad K_{ij}^{13} = K_{ij}^{14} = 0,$$

$$K_{ij}^{21} = \int_{\eta_e}^{\eta_{e+1}} A \psi_i \bar{h} \psi_j d\eta, \quad K_{ij}^{22} = -\int_{\eta_e}^{\eta_{e+1}} \left(\frac{\partial \psi_i}{\partial \eta} \frac{\partial \psi_j}{\partial \eta} - \psi_i \eta \frac{\partial \psi_j}{\partial \eta} - \psi_i \psi_j + A \psi_i \bar{h} \psi_j \right) d\eta$$

$$K_{ij}^{23} = K_{ij}^{24} = K_{ij}^{31} = K_{ij}^{32} = 0,$$

$$K_{ij}^{33} = -\int_{\eta_e}^{\eta_{e+1}} \left(\frac{\partial \psi_i}{\partial \eta} \frac{\partial \psi_j}{\partial \eta} - A \Pr \psi_i \bar{f} \frac{\partial \psi_j}{\partial \eta} - \Pr Nt \psi_i \bar{\theta}' \frac{\partial \psi_j}{\partial \eta} - \Pr \psi_i \frac{\eta}{2} \frac{\partial \psi_j}{\partial \eta} \right) d\eta,$$

$$K_{ij}^{34} = \int_{\eta_e}^{\eta_{e+1}} Nb \Pr \psi_i \bar{\theta}' \frac{\partial \psi_j}{\partial \eta} d\eta, \qquad K_{ij}^{41} = K_{ij}^{42} = 0,$$

$$K_{ij}^{43} = -\int_{\eta_e}^{\eta_{e+1}} \frac{Nt}{Nb} \frac{\partial \psi_i}{\partial \eta} \frac{\partial \psi_j}{\partial \eta} d\eta, \quad K_{ij}^{44} = -\int_{\eta_e}^{\eta_{e+1}} \left(\frac{\partial \psi_i}{\partial \eta} \frac{\partial \psi_j}{\partial \eta} - ALe \psi_i \bar{f} \frac{\partial \psi_j}{\partial \eta} - Le \psi_i \frac{\eta}{2} \frac{\partial \psi_j}{\partial \eta} \right) d\eta$$

$$b_i^1 = 0, \ b_i^2 = -\int_{\eta_e}^{\eta_{e+1}} \psi_i (A - 1) d\eta - \left(\psi_i \frac{\partial h}{\partial \eta} \right)_{\eta_e}^{\eta_{e+1}}, \ b_i^3 = -\left(\psi_i \frac{\partial \theta}{\partial \eta} \right)_{\eta_e}^{\eta_{e+1}}, \ b_i^4 = -\left(\psi_i \frac{\partial \phi}{\partial \eta} \right)_{\eta_e}^{\eta_{e+1}}$$

where

$$\bar{f} = \sum_{i=1}^{2} \psi_i \bar{f}_i, \quad \bar{g} = \sum_{i=1}^{2} \psi_i \bar{g}_i, \quad \bar{\theta} = \sum_{i=1}^{2} \psi_i \bar{\theta}_i, \quad \bar{\theta}_i = \sum_{i=1}^{2} \frac{\partial \psi_i}{\partial \eta} \bar{\theta}_i, \quad \bar{\phi} = \sum_{i=1}^{2} \psi_i \bar{\phi}_i,$$

Each element matrix is of the order 8×8. The entire flow domain is divided into a set of finite uniform two nodes line elements and following the assembly of all the elements equations, a global system is generated. The resulting global system of equations is non-linear, therefore an iterative scheme is used for solving it. The system is linearized by incorporating the functions $\overline{f}$, $\overline{g}$, $\overline{\theta}$ and $\overline{\phi}$, which are assumed to be known. After imposing the boundary conditions, remaining transformed linear equations are solved by using Gauss elimination method by maintaining an accuracy of 0.0001. A convergence criterion based on the relative difference between the current and previous iterations is employed. When these differences reach to the desired accuracy, the solution is assumed to have converged and iterative process is terminated. The Gaussian quadrature is used for solving the integrations.

4 Results and Discussion

Numerical solutions to the governing ordinary differential Eqs (7-9) with the corresponding boundary conditions Eq. (10) were obtained using finite element method (FEM). For solving this problem with FEM, we have to choose a suitable value of η_∞ (where η_∞ correspond to $\eta\to\infty$) and step size (h) which satisfy all boundary conditions and to give a better approximation for the solution. Care has been taken in choosing η_∞ for a given set of parameters because for a fixed value of η_∞ for all calculations may produce inaccurate results. In this problem, we observe that dual solutions exist, one representing attached flow, the other for reversed flow, which is identical to the solution obtained by Ma and Hui[13] for a classical viscous fluid, and thus gives confidence that the numerical results in our case are accurate.

To determine the suitable step size (*h)*, computations have been performed with different values of step size $(h=0.5,\ 0.1,\ 0.01,\ 0.005,\ 0.004)$ as shown in Table 1. We observe that very slight change occurs after $h=0.005$, but the computational time increases too much. Thus, for the computational purpose $h=0.005$ is taken for presentation of the results. Table 2 shows the comparison of the present numerical results with those of Bejan[9] for the solutions of Eqs (16-18), which shows a favorable agreement. Therefore, we are confident that the present results are correct and accurate.

Variations of the reduced skin friction coefficient $f''(0)$, the reduced local Nusselt number $-\theta'(0)$ and the reduced local Sherwood number $-\varphi'(0)$ as a function of the suction/injection parameter s under different values of the unsteadiness parameter (A) are shown in Figs 1-3. It is interesting that there are two solution branches, which are labeled in the plots by first (upper branch) and second (lower branch) solutions for each value of s under the same value of unsteadiness parameter (A) for $s>s_c$, where $s_c<0$ is the critical value of s at which the two solution branches meet with each other. Based on our computation, the critical value $s_c<0$ increases as we increase the value of unsteadiness parameter (A). It means that the range of the suction/injection

Table 2 – Comparison of the present results with those of Bejan[9]

	Pr	Bejan[9]	Present results
$f''(0)$		1.233	1.2326
$-\theta'(0)$	0.7	0.496	0.4963
	0.8	0.523	0.5229
	1	0.570	0.5705
	5	1.043	1.0434
	10	1.344	1.3388

Table 1—Calculation of skin friction coefficient, Nusselt number and Sherwood number when $Nb=0.5,\ Nt=0.5,\ Pr=1,\ Le=2.0,\ A=1,\ s=1.0$

Step size	$\lvert-f''(0)\rvert$		$\lvert-\theta'(0)\rvert$		$\lvert-\phi'(0)\rvert$	
h	1st Sol	2nd Sol	1st Sol	2nd Sol	1st Sol	2nd Sol
0.5	1.5608	2.3344	0.9605	0.4454	1.7128	1.0212
0.1	1.6438	2.5794	0.8929	0.4819	2.0343	1.2604
0.01	1.6587	2.6306	0.8975	0.4897	2.0780	1.2943
0.005	1.6597	2.6334	0.8980	0.4902	2.0797	1.2957
0.004	1.6599	2.6339	0.8981	0.4903	2.0799	1.2959

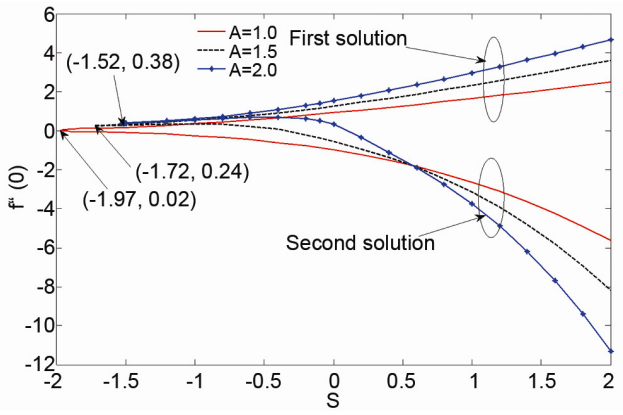

Fig. 1 – Variation of $f''(0)$ with s for various values of A when Nb = 0.5, Nt = 0.5, Pr = 1.0, Le = 2.0

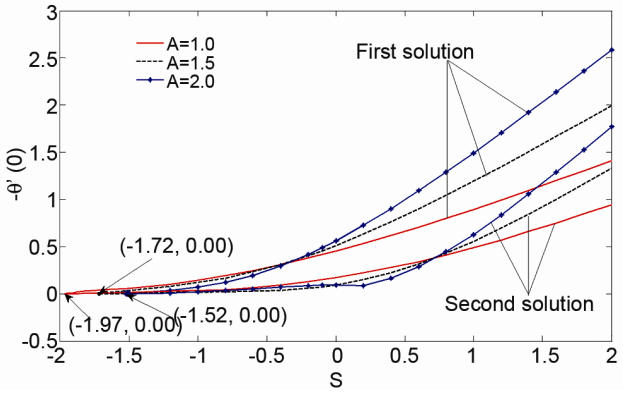

Fig. 2 – Variation of $-\theta'(0)$ with s for various values of A when Nb = 0.5, Nt = 0.5, Pr = 1.0, Le = 2.0

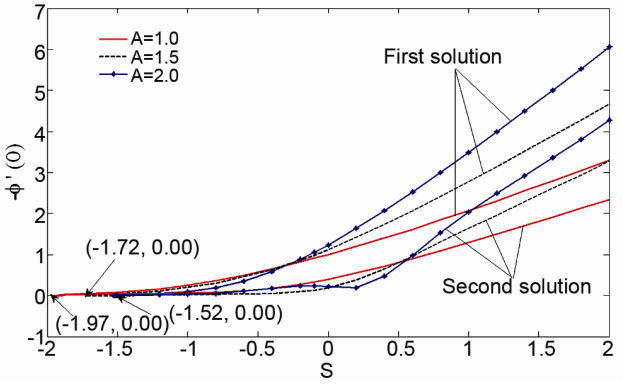

Fig. 3 – Variation of $-\phi'(0)$ with s for various values of A when Nb = 0.5, Nt = 0.5, Pr = 1.0, Le = 2.0

parameter s for which the solution exists decreases with increasing A. For the first solution branch, $f''(0)$, $-\theta'(0)$ and $-\phi'(0)$ monotonically decrease with decreasing s. Thus, the surface shear stress, heat transfer and mass transfer rate at the surface is higher for suction $(s > 0)$ compared to injection $(s < 0)$.

The second solution branch, however, shows more complicated and quite different behaviors compared with the first solution branch. The values of $f''(0)$, $-\theta'(0)$ and $-\phi'(0)$ for the first solution branch are always higher than the second solution branch. For the second solution, with the increase in A, $f''(0)$ decreases, while for $s < 0.5$ the pattern is reversed. There exist crossovers among different solution curves of $-\theta'(0)$ and $-\phi'(0)$ for different values of A. Mathematically, we postulate that both solution branches are valid solutions, but physically the second solution branch may not be feasible (realizable) in practice. Merkin[48], Weidman *et al.*[49] and very recently Postelnicu and Pop[50] have shown that the first solution branch is linearly stable and physically realizable.

Figures 4-12 present the velocity, temperature and nanoparticle volume fraction profiles for various values of parameters. It is seen that all of these figures satisfy the boundary conditions Eq. (20), thus support the validity of the present results, besides supporting the dual nature of the solutions shown in Figs 1-3. Figure 4 shows that the velocity gradient at the surface is positive for the first solution and negative for the second solution, which is in agreement with the result presented in Fig. 1. For the first solution, which we expect to be the physically feasible solution, the velocity increases as A increases, as a result velocity gradient at the surface increases, and in consequent increase the skin friction coefficient. We also observed that the boundary layer become thinner for a value of A with large magnitude. Figure 5 shows that temperature (temperature gradient) decreases (increases) with increasing A. The same behavior is observed in the nanoparticle volume fraction profiles shown in Fig. 6. Further, the solution on the lower branch for both suction parameter (s) and unsteadiness parameter (A) has a region of reversed flow (i.e., $f'(\eta) < 0$), which is physically inappropriate and is also consider as an indication that the flow is unstable (Ridha[51]). Figure 8 exhibits that the temperature in the boundary layer decreases with an increase in s. Thus, suction plays an important role in enhancing the heat transfer rate.

Figures 9 and 10 depict the effect of Lewis number on the variation of temperature and nanoparticle

concentration in the boundary layer. These figures show that the Lewis number significantly affects the concentration distribution (Fig. 10), but has little influence on the temperature distribution (Fig. 9). Lewis number defines the ratio of thermal diffusivity to mass diffusivity. Therefore, for a base fluid of certain kinematic viscosity, a higher Lewis number implies a lower Brownian diffusion coefficient which result in a shorten penetration depth for the concentration boundary layer, which we can see in Fig. 10.

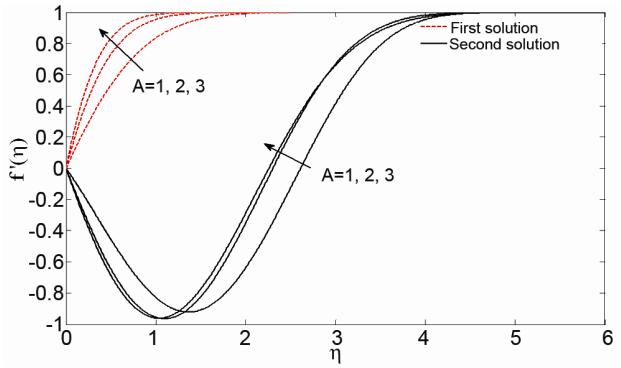

Fig. 4 – Velocity profile for various values of A when Nb = 0.5, Nt = 0.5, Pr = 1.0, Le = 2.0, S=0.5

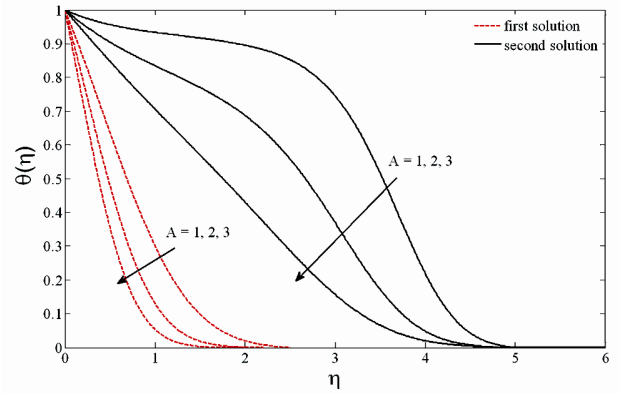

Fig. 5 – Temperature profile for various values of A when Nb = 0.5, Nt = 0.5, Pr = 1.0, Le = 2.0, S=0.5

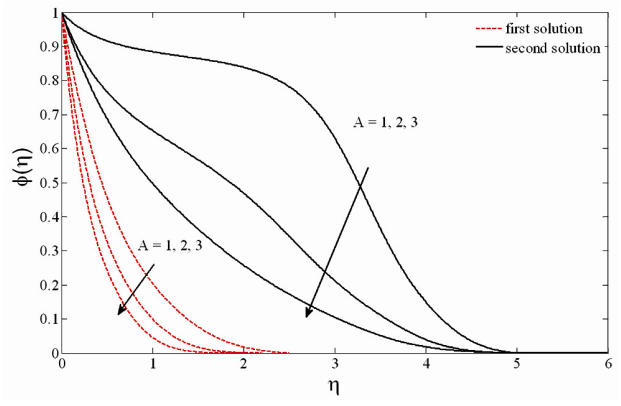

Fig. 6 – Concentration profile for various values of A when Nb = 0.5, Nt = 0.5, Pr = 1.0, Le = 2.0, S=0.5

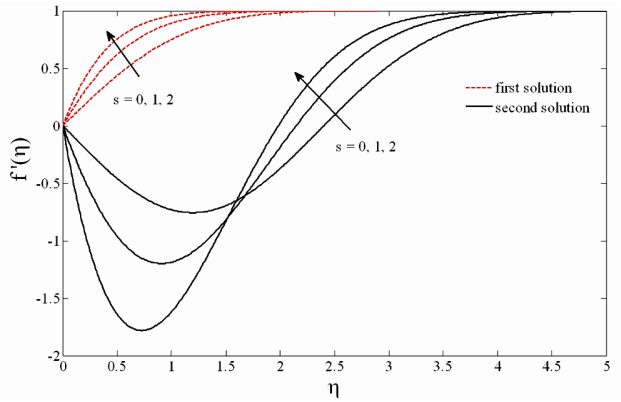

Fig. 7 – Velocity profile for various values of s when Nb = 0.5, Nt = 0.5, Pr = 1.0, Le = 2.0, A=1.0

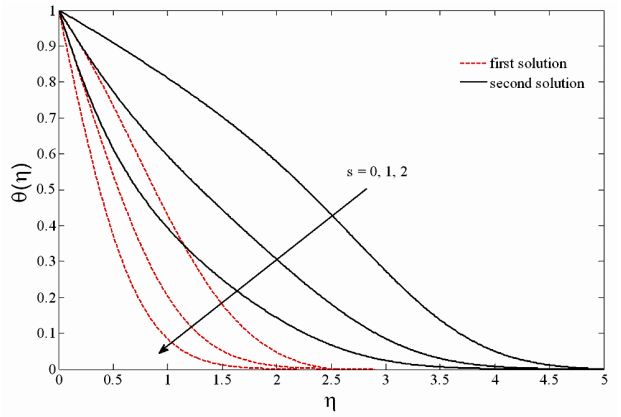

Fig. 8 – Temperature profile for various values of s when Nb = 0.5, Nt = 0.5, Pr = 1.0, Le = 2.0, A=1.0

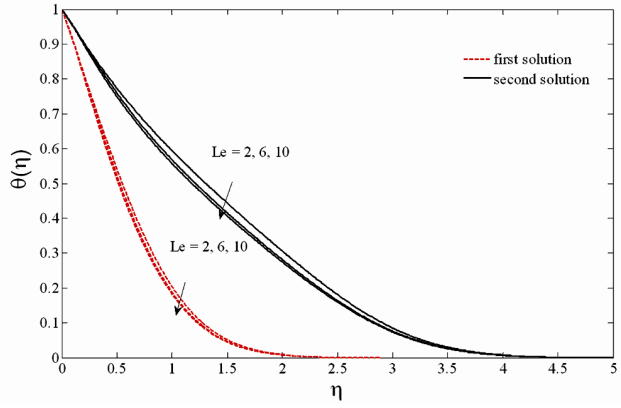

Fig. 9 – Temperature profile for various values of Le when Nb = 0.5, Nt = 0.5, Pr = 1.0, S = 1.0, A=1.0

Finally, Figs 11 and 12 show the temperature distribution in the thermal boundary layer for different values of Brownian motion and thermophoretic parameters. Brownian motion and thermophoretic effects serve to warm the boundary layer, which is clearly visible from these figures.

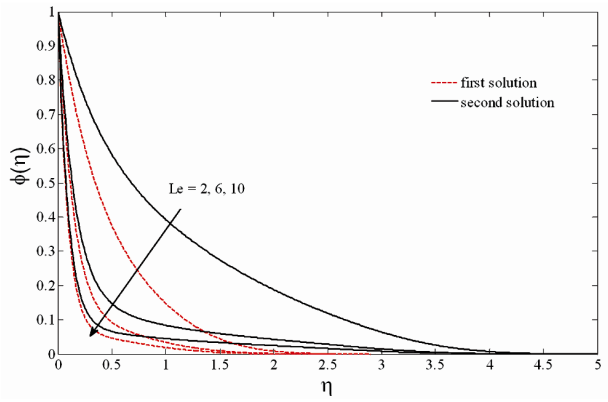

Fig. 10 – Concentration profile for various values of Le when Nb = 0.5, Nt = 0.5, Pr = 1.0, S = 1.0, A=1.0

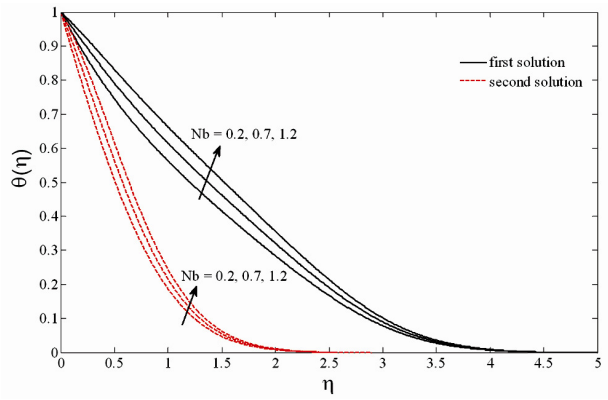

Fig. 11 – Temperature profile for various values of Nb when Nb = 0.5, Nt = 0.5, Pr = 1.0, S = 1.0, A=1.0

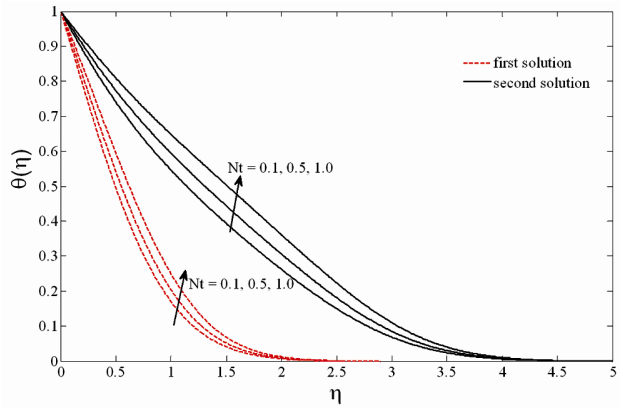

Fig. 12 – Temperature profile for various values of Nt when Le = 2.0, Nb = 0.5, Pr = 1.0, S=1.0, A=1.0

5 Conclusions

In this paper, the problem of two-dimensional stagnation point flow of a viscous and incompressible nanofluid over a permeable flat plate is studied. The governing partial differential equations for mass, momentum, energy and nanoparticles conservation are transformed into ordinary differential equations using a similarity transformation. These equations were solved numerically using finite element method. We found that there are two solution branches for different boundary layer thickness. The results also indicate that unsteadiness parameter reduce the range of the suction/injection parameter for which the solution exists. Brownian motion and thermophoretic effects serve to warm the boundary layer, while suction effect reduces the temperature inside the boundary layer.

Acknowledgement

This work was supported by Research Grants from Science and Engineering Research Board, Department of Science & Technology, Govt. of India (Project Code: ECR/2016/000368), the Ministry of Higher Education, Malaysia (Project Code: FRGS/1/2012/SG04/UKM/01/1) and the Universiti Kebangsaan Malaysia (Project Code: DIP-2012-31).

Nomenclature

A	constant
c	volumetric volume expansion
C	nanoparticle fraction
C_f	skin friction coefficient
C_w	nanoparticle volume fraction at the plate
C_∞	ambient nanoparticle volume fraction
D_B	Brownian diffusion coefficient
D_T	thermophoretic diffusion coefficient
f	dimensionless stream function
j_w	concentration flux at the plate
k	thermal conductivity
Le	Lewis number
Nb	Brownian motion parameter
Nt	thermophoresis parameter
Nu_x	local Nusselt number
Pr	Prandtl number
q_w	heat flux at the plate
Re_x	local Reynolds number
Sh_x	local Sherwood number
t	time
T	temperature
T_w	temperature at the plate

T_∞ ambient temperature
u, v velocity components along $x-$ and $y-$ axes
u_e velocity of the free stream
v_w mass flux velocity
x, y cartesian coordinate measured along the surface and normal to it, respectively

Greek symbols
α thermal diffusivity
ϕ dimensionless nanoparticle fraction
η similarity variable
μ dynamic viscosity
θ dimensionless temperature
ρ_f fluid density
ρ_p nanoparticle mass density
$(\rho c)_f$ heat capacity of the fluid
$(\rho c)_p$ effective heat capacity of the nanoparticle material
τ heat capacity ratio
ν kinematic viscosity
ψ free stream function

References

1 Hiemenz K, *Dingler Polytech J*, 326 (1911) 321.
2 Homann F, *Z Angew Math Mech*, 16 (1936) 153.
3 Ariel P D, *J Appl Mech*, 61 (1994) 976.
4 Burde G I, *ASME J Fluids Eng*, 117 (1995) 189.
5 Massoudi M & Ramezan M, *Proc ASME Heat Trans Div*, 130 (1990) 81.
6 Massoudi M & Ramezan M, *Mech Res Commun*, 19 (1992) 129.
7 Garg V K, *Acta Mech*, 104 (1994) 159.
8 Chiam T C, *Int Commun Heat Mass Trans*, 23 (1996) 239.
9 Bejan A, *Convection Heat Transfer*, (Wiley, New Jersey), 2004.
10 Schlichting H & Gersten K, *Boundary-Layer Theory*, (Springer, New York), 2000.
11 Leal L G, *Advanced transport phenomena: fluid mechanics and convective transport processes*, (Cambridge University Press, Cambridge), 2007.
12 Pop I & Ingham D B, *Convective heat transfer: mathematical and computational modelling of viscous fluids and porous media*, (Pergamon, Oxford), 2001.
13 Ma P K H & Hui W H, *J Fluid Mech*, 216 (1990) 537.
14 Telionis D P, *Unsteady Viscous Flows*, (Springer, New York), 1981.
15 Choi S U S, *Enhancing thermal conductivity of fluids with nanoparticles. In: developments and application of non-newtonian flows*. FED-vol. 231/MD-vol. 66 (1995) 99.
16 Kakaç S, *Int J Heat Mass Trans*, 52 (2009) 3187.
17 Das S K, Choi S U S, Yu W & Pradet T, *Nanofluids: Science and technology*, (Wiley, New Jersey), 2007.
18 Trisaksri V & Wongwises S, *Renew Sust Energ Rev*, 11 (2007) 512.
19 Wang X-Q & Mujumdar A S, *Int J Thermal Sci*, 46 (2007) 1.
20 Lee J H, Lee S H, Choi C J, Jang S P & Choi S U S, *Int J Micro-Nano Scale Transp*, 1 (2010) 269.
21 Eagen J, Rusconi R, Piazza R & Yip S, *ASME J Heat Trans*, 132 (2010) 102402.
22 Wong K F V & Leon O D, *Adv Mech Eng*, 2010 (2010) 519659.
23 Fan J & Wang L, *ASME J Heat Trans*, 133 (2011) 040801.
24 Buongiorno J, *ASME J Heat Trans*, 128 (2006) 240.
25 Tiwari R K & Das M K, *Int J Heat Mass Trans*, 50 (2007) 2002.
26 Nield D A & Kuznetsov A V, *Int J Heat Mass Trans*, 52 (2009) 3187.
27 Nield D A & Kuznetsov A V, *Int J Heat Mass Trans*, 54 (2011) 374.
28 Nield D A & Kuznetsov A V, *Int J Heat Mass Trans*, 52 (2009) 5796.
29 Kuznetsov A V & Nield D A, *Int J Therm Sci*, 49 (2010) 243.
30 Kuznetsov A V & Nield D A, *Int J Therm Sci*, 50 (2011) 712.
31 Kuznetsov A V & Nield D A, *Transp Porous Med*, 81 (2010) 409.
32 Bachok N, Ishak A & Pop I, *Int J Therm Sci*, 49 (2010) 1663.
33 Bachok N, Ishak A & Pop I, *Int J Heat Mass Trans*, 55 (2012) 2102.
34 Alsaedi A, Awais M & Hayat T, *Commun Nonlinear Sci Numer Simulat*, 17 (2012) 4210.
35 Hamad M A A & Ferdows M, *Commun Nonlinear Sci Numer Simulat*, 17 (2012) 132.
36 Abu-Nada E, *Int J Heat Fluid Flow*, 29 (2008) 242.
37 Muthtamilselvan M, Kandaswamy P & Lee J, *Commun Nonlinear Sci Numer Simulat*, 15 (2010) 1501.
38 Abu-Nada E & Oztop H F, *Int J Heat Fluid Flow*, 30 (2009) 669.
39 Talebi F, Houshang A & Shahi M, *Int Commun Heat Mass Trans*, 37 (2010) 79.
40 Bachok N, Ishak A & Pop I, *Physica B*, 406 (2011) 1767.
41 Bachok N, Ishak A, Nazar R & Pop I, *Physica B*, 405 (2010) 4914.
42 Bachok N, Ishak A & Pop I, *Int J Heat Mass Trans*, 55 (2012) 642.
43 Kuznetsov A V & Nield D A, *Int J Therm Sci*, 49 (2010) 243.
44 Reddy J N, *An introduction to the finite element method*, (McGraw-Hill, New York), 1984.
45 Bhargava R, Sharma R & Beg O A, *Int J Appl Math Mech*, 5 (2009) 15.
46 Sharma R, Bhargava R & Bhargava P, *Comput Mater Sci*, 48 (2010) 537.
47 Sharma R, *Appl Math Comput*, 219 (2012) 976.
48 Merkin J H, *J Eng Math*, 20 (1985) 171.
49 Weidman P D, Kubitschek D G & Davis A M J, *Int J Eng Sci*, 44 (2006) 730.
50 Postelnicu A & Pop I, *Appl Math Comput*, 217 (2011) 4359.
51 Ridha A, *Int J Eng Sci*, 34 (1996) 659.